Published in final edited form as:

Chem Biol. 2014 March 20; 21(3): 422–429. doi:10.1016/j.chembiol.2014.01.012.

MRI-based detection of alkaline phosphatase gene reporter activity using a porphyrin solubility switch

Gil G. Westmeyer[1,2,3], **Elena G. Emer**[1], **Jutta Lintelmann**[4], and **Alan Jasanoff**[1,†]

[1]Departments of Brain & Cognitive Sciences, Biological Engineering, and Nuclear Science & Engineering, Massachusetts Institute of Technology, 77 Massachusetts Ave., Rm. 16-561, Cambridge, MA 02139, USA

[2]Department of Nuclear Medicine, Technische Universität München, 81675 Munich, Germany

[3]Institute of Biological and Medical Imaging and Institute of Developmental Genetics

[4]Comprehensive Molecular Analytics Cooperation Group, Helmholtz Zentrum München, German Research Center for Environmental Health, 85764 Munich/Neuherberg, Germany

SUMMARY

The ability to map patterns of gene expression noninvasively in living animals could have impact in many areas of biology. Reporter systems compatible with magnetic resonance imaging (MRI) could be particularly valuable, but existing strategies tend to lack sensitivity or specificity. Here we address the challenge of MRI-based gene mapping using the reporter enzyme secreted alkaline phosphatase (SEAP), in conjunction with a water soluble metalloporphyrin contrast agent. SEAP cleaves the porphyrin into an insoluble product that accumulates at sites of enzyme expression and can be visualized by MRI and optical absorbance. The contrast mechanism functions *in vitro*, in brain slices, and in animals. The system also provides the possibility of readout both in the living animal and by *post mortem* histology, and it notably does not require intracellular delivery of the contrast agent. The solubility switch mechanism used to detect SEAP could be adapted for imaging of additional reporter enzymes or endogenous targets.

INTRODUCTION

Magnetic resonance imaging (MRI) provides exceptional ability to visualize soft tissue contrast at submillimeter resolution in intact human and animal subjects. Although MRI offers powerful functionality for anatomical analysis and functional studies based on blood flow, application of MRI for monitoring molecular-level processes remains challenging due to the relative insensitivity of MRI to molecular imaging probes (Lelyveld et al., 2010). Canonical MRI contrast agents derived from paramagnetic complexes that alter longitudinal

†address correspondence to: AJ, jasanoff@mit.edu.

(T_1) magnetic resonance relaxation times are difficult to detect at concentrations below 10 μM, whereas most clinically or biologically interesting target analytes are present at much lower levels, often in the nanomolar or subnanomolar range. In part for this reason, there has been considerable interest in exploring strategies for amplifying the contrast arising from molecular species in MRI (Hsieh and Jasanoff, 2012; Tu et al., 2011).

Enzymes are widely used to amplify molecular signals, both in nature and in a broad array of biological assays. Prominent examples of enzymatic strategies in conventional histology and light microscopy include the use of β-galactosidase (β-gal) (Goring et al., 1987), luciferase (DiLella et al., 1988) and other proteins as reporter genes, and the application of horseradish peroxidase (Nakane and Pierce, 1966) and alkaline phosphatase (Avrameas, 1969) conjugates for immunodetection. Strategies for detection of enzymes in MRI are less developed but actively researched. One of the first instances of reporter enzyme detection in MRI employed a gadolinium-based T_1 contrast agent that undergoes an increase in potency following cleavage by β-gal (Louie et al., 2000); further MRI-detectable β-gal substrates have since been introduced (Arena et al., 2011; Cui et al., 2010; Keliris et al., 2011). Additional strategies for enzyme detection by MRI have employed molecular mechanisms that lead to local accumulation of paramagnetic species such as iron ions, iron oxide nanoparticles, and gadolinium complexes [reviewed in (Westmeyer and Jasanoff, 2007)]. Although a number of proofs of concept have been produced using these approaches in cell culture and live organisms, few approaches have been applied in subsequent studies and there is a need for continued improvement and innovation in this research area.

In recent work we presented a system for detecting activity of a secreted enzymatic reporter in MRI (Westmeyer et al., 2010). By harnessing an extracellular enzyme, the secreted alkaline phosphatase (SEAP) (Berger et al., 1988), we obviated the need for intracellular delivery of an MRI contrast agent, which can be a substantial hurdle for *in vivo* imaging studies. We detected an SEAP product by using an MRI contrast agent sensor, rather than by using a contrast agent as a substrate itself. Advantages of this strategy are that it is reversible upon product removal and that the contrast agent is not used up, but a disadvantage is the complexity of the detection mechanism, which requires delivery both of an SEAP substrate and of a supramolecular iron oxide-based MRI sensor to their sites of action. We therefore sought a simpler mechanism for our initial efforts to detect SEAP activity by MRI *in vivo*. Paramagnetic manganese porphyrins are among the strongest contrast agents for T_1-weighted MRI (Chen et al., 1984; Koenig et al., 1987), and we showed in another study (Lee et al., 2010) that labile zinc binding by an anionic porphyrin-based molecular imaging agent (Zhang et al., 2007) promotes localization of the probe in tissue, probably because of a change in the charge of the complex. We reasoned that an anionic phosphoporphyrin designed to be a substrate for SEAP could undergo a phosphatase-catalyzed solubility switch (Yao et al., 2007) and accumulate similarly in the presence of SEAP reporter expression (Figure 1). Visualization of the product would then occur following depletion of the soluble starting material, which would be expected to wash out within several hours *in vivo* (Lee et al., 2010). The mechanism of contrast induction in this scenario parallels approaches used successfully to detect tumor-associated proteases in cancer models (Lepage et al. 2007; Gringeri et al. 2012). Here we evaluate SEAP in combination with a solubility-

switching porphyrin substrate *in vitro* and in intact tissue, and provide indication of the potential utility of this strategy for reporter enzyme monitoring by MRI and optical histology.

RESULTS

A phosphorylated metalloporphyrin, manganese(III)-tetraphenylporphyrin phosphate (Mn-$TPPP_4$), was synthetized and characterized *in vitro*. The unmetallated version of this compound has been shown previously to act as a substrate for tissue-nonspecific alkaline phosphatase (Kawakami and Igarashi, 1995), and the axial *p*-phosphophenyl groups of $TPPP_4$ are structurally similar to the promiscuous phosphatase substrate *p*-nitrophenylphosphate (Hudson et al., 1947), known to be cleaved by secreted alkaline phosphatase (SEAP), and its membrane-anchored placental isoform (PLAP). Mn-$TPPP_4$ was therefore expected be progressively dephosphorylated, via tri-, bis-, and monophos-phate intermediates, to manganese(III)-tetrahydroxyphenylporphyrin (Mn-THPP), a compound containing four axial *p*-hydroxyphenyl groups. Varying concentrations of Mn-$TPPP_4$ (6–191 μM) in 100 μL volumes were incubated with 0.01 units of PLAP (~10 pmol) from a commercial source and assayed optically and by MRI. In fact, Mn-$TPPP_4$ underwent a sharp change in solubility in the presence of PLAP, forming a dark green precipitate that could be removed from suspension by centrifugation (Figure 2A). Precipitation did not occur when a control protein, bovine serum albumin (BSA), was added in place of PLAP. The phosphatase-dependent solubility change of the porphyrin agent was accompanied by a spectral change resulting in a shift of λ_{max} from 469 to 476 nm (Figure 2B). The time course of enzymatic dephosphorylation was also followed via liquid chromatography-mass spectrometry, which showed increasing accumulation of partially dephosphorylated product (*m/z* = 811 for Mn-TPPP monoester) and completely dephosphorylated product (*m/z* = 731 for Mn-THPP) over a 60 minute period (Supplemental Figure S2). The buildup of these species also corresponded inversely to the time course of material remaining in solution over time, as judged by optical absorbance of reaction mixture supernatants sampled over the same period (correlation coefficients > 0.9, $p < 0.01$).

MRI properties of a solution of Mn-$TPPP_4$ also changed upon addition of PLAP. Prior to addition of enzyme, Mn-$TPPP_4$ modulated the T_1 relaxation rate (R_1) according to its relaxivity (r_1, slope of R_1 *vs.* concentration) of 6.1 ± 0.07 $mM^{-1}s^{-1}$. The observed R_1 was dramatically affected by addition of PLAP, however, due primarily to enzyme-catalyzed precipitation. When 0.01 units of enzyme were added to a 127 μM solution of Mn-$TPPP_4$ and incubated for 30 min., R_1 of the mixture was 0.29 ± 0.01 s^{-1}. Incubation with an equivalent amount of BSA led to a substantially larger R_1 of 0.76 ± 0.05 s^{-1}. Similar relaxation differences were observed for lower concentrations of Mn-$TPPP_4$ (Figure 2C), and linearity of R_1 values *vs.* [Mn-$TPPP_4$] in both PLAP and BSA supplemented conditions indicated that observed relaxation rate changes were due to the action of the phosphatase, rather than spontaneous precipitation of the contrast agent. According to this analysis, the apparent r_1 of the enzymatically dephosphorylated porphyrin species was 2.4 ± 0.1 $m^{-1}s^{-1}$, a reduction by more than 50% compared with r_1 of the untreated substrate. We also compared apparent relaxivity measurements in pH 4.5 buffers designed to mimick endocytic conditions and found no significant differences from those recorded at pH 7 (see Methods).

These results suggest that enzyme-catalyzed dephosphorylation of Mn-$TPPP_4$ should also be detectable as T_1 contrast changes in MRI scans in cellular environments.

As an initial test of the Mn-$TPPP_4$ solubility switch mechanism in a biological context, we examined the effect of expressing SEAP in cell culture on the behavior of Mn-$TPPP_4$ in culture supernatants. HEK293 cells were transfected with DNA constructs directing expression of SEAP or enhanced yellow fluorescent protein (EYFP). Following coincubation of the cells with 13 μM Mn-$TPPP_4$ for ≥ 2.5 hrs. in media, supernatant fractions were withdrawn and analyzed. As with the addition of purified enzyme, SEAP secretion into culture medium induced formation of a precipitate that could be pelleted by centrifugation (Supplemental Figure S1A). Formation of this precipitate also resulted in a change in T_1-weighted MRI signal and a decrease in R_1 (Supplemental Figure S1B), with respect to control conditions. The fact that observed changes were minor in the presence of cells expressing EYFP in place of SEAP suggests that Mn-$TPPP_4$ turnover should permit relatively specific detection of the SEAP reporter in biologically complex environments.

SEAP/PLAP has been used previously as a marker in histological studies of gene expression in the rodent central nervous system (DePrimo et al., 1996; Fields-Berry et al., 1992). As a proof-of-principle of the Mn-$TPPP_4$ solubility switch mechanism for gene expression mapping by MRI, we therefore investigated whether the compound could detect SEAP expression in genetically modified rat brain slices. Sprague Dawley rats were injected in the right and left thalamus with adeno-associated viral vectors (AAV9) driving SEAP or control gene (GFP) expression from constitutive cytomegalovirus promoters. Three to six weeks after infection, animals were sacrificed and brains were removed and processed by standard techniques used previously for histochemical analysis of SEAP expression. Brain slices were subjected to uniform staining with Mn-$TPPP_4$ and then visualized by MRI and light microscopy. *Ex vivo* MRI was performed with a custom surface coil on a 9.4 T scanner, using a two dimensional T_1-weighted spin echo pulse sequence with 100 μm in-plane resolution and repetition and echo times (*TR* and *TE*) equal to 100 and 12 ms, respectively. Brain slices adjacent to the ones used for MRI scanning were treated with 5-bromo-4-chloro-3-indoylphosphate (BCIP) and nitro-blue tetrazolium (NBT), a chromogenic combination of reagents that forms a dark purple precipitate in the presence of alkaline phosphatase activity and is conventionally used for visualization of SEAP expression patterns.

Figure 3 shows representative MRI and optical results. A clear T_1-weighted hyper-intensity is found near the coordinates of AAV9-SEAP viral deposition in panel A, whereas T_1 enhancement is not visible on the contralateral side where control virus was delivered. Analysis of the raw signal intensities (panel B) shows that the MRI intensity on the hyperintense side is roughly two times the signal level seen on the control side. Accumulation of the contrast agent is also visible optically, because of the strong absorbance of Mn-$TPPP_4$ and its dephosphorylated analogs. Panel C shows a light micrograph of the same brain slice scanned for panel A. The strong, dark green staining visible on the right side is similar in color to the precipitates visible in the *in vitro* experiments of Figure 2 and Figure S1, and corresponds spatially to the hyperintensity detected by MRI. This indicates that the MRI contrast observed in this experiment most

likely arises directly from localized accumulation of the dephosphorylated contrast agent near the injection site for the SEAP-expressing viral vector, despite the fact that the entire brain slice was exposed to Mn-$TPPP_4$ prior to imaging. Evaluation of SEAP expression profiles by the BCIP-NBT staining method (Figure 3D) reveals a largely similar pattern of staining. The correspondence of BCIP-NBT and MRI results further supports the validity of the MRI-based SEAP imaging approach, and indicates that the MRI method resolves SEAP activity with efficacy comparable to the established histological method.

To address the ability of the Mn-$TPPP_4$ solubility switch mechanism for detecting SEAP expression *in vivo*, we combined viral injection with local delivery of the contrast agent by intracranial injection into live rat brains. Approximately ten weeks after stereo-taxic injection of viruses encoding SEAP or GFP (control) into thalamic targets, animals were anesthetized with isoflurane and infused with 6 μL of 635 μM Mn-$TPPP_4$ in artificial cerebrospinal fluid (aCSF). Within two hours of contrast agent injection, animals were scanned using a cross coil radiofrequency apparatus on a 4.7 T MRI scanner (fast low-angle shot pulse sequence, 50/5 ms *TR*/*TE*, 250 μm isotropic resolution). Further scan sessions were performed on subsequent days after Mn-$TPPP_4$ delivery. After the last imaging session, animals were sacrificed and brain slices prepared for visualization by optical absorbance and BCIP-NBT staining. Histological slices showed no evidence of tissue toxicity in brain volumes filled with porphyrin or associated with elevated BCIP-NBT reactivity. MRI scans were analyzed, following earlier procedures from our lab, by defining cylindrical regions of interest (ROIs) with a diameter and length of 1.75 mm near the contrast agent injection sites and evaluating mean signal intensity normalized by signal intensity in control regions lateral to the test areas.

A sample image series is shown in Figure 4A. Bilateral signal increases are apparent, but with greater MRI signal near the injection site pretreated with AAV9-SEAP. Signal increases observed on both SEAP-expressing and control sides decrease over time following contrast agent delivery, with consistently higher MRI signal remaining in the SEAP-expressing hemisphere throughout the time course. These MRI enhancements were consistent with post-mortem examination of BCIP-NBT and Mn-$TPPP_4$ staining patterns (panel B). Panel C shows group data obtained from five AAV9-SEAP injection sites, three AAV9-GFP control sites, and two vehicle control sites. Average MRI signal amplitudes were computed over peri-injection ROIs, and normalized by the mean signal in neighboring ROIs that did not receive contrast agent injections. Approximately two hours after Mn-$TPPP_4$ injection, relative MRI signal in SEAP-expressing brain regions was 41 ± 4% above baseline, whereas relative signal in GFP-expression regions was 19 ± 9% above baseline and relative signal at vehicle control sites was 9 ± 9%; the reporter-dependent difference was statistically significant with *t*-test $p < 0.04$ compared with each control. Two days after contrast agent infusion, relative MRI signal in SEAP, GFP, and vehicle sites was 21 ± 3%, 9 ± 5%, and 6 ± 7% respectively, reflecting weakening of the contrast difference over time.

The differences between contrast time courses observed following Mn-$TPPP_4$ injection in the absence *vs.* presence of SEAP expression could also be mimicked in untransduced rats by control injections of the fully dephosphorylated product Mn-THPP (solubilized at pH 14) and of an uncleavable Mn-$TPPP_4$ analog, Mn(III)-*meso*-tetrakis(4-

sulfonatophenyl)porphyrin (Mn-$TPPS_4$), in which the phosphates of Mn-$TPPP_4$ are replaced by sulfonate groups; this further validates the proposed mechanism for contrast agent accumulation in the presence of SEAP (Supplemental Figure S3). The ability of Mn-THPP to induce T_1 contrast enhancement, despite its relative insolubility, was consistent with its *in vitro* relaxivity of $0.82 \pm 0.02\ m^{-1}s^{-1}$, measured under conditions of the intracerebral injection in aCSF, pH 14. As a test for the influence of endogenous phosphatase activity on the observed MRI contrast patterns, Mn-$TPPP_4$ was injected in the absence or presence of 5 mM sodium orthovanadate, a phosphatase inhibitor with submicromolar inhibition constants for tissue-nonspecific alkaline phosphatases. No significant phosphatase inhibitor-dependent contrast differences were observed (Supplemental Figure S4). These experiments therefore collectively show that the Mn-$TPPP_4$ solubility switch mechanism permits specific detection of SEAP reporter expression *in vivo*. Although unbiased spatial mapping of SEAP activity patterns across the entire brain would require trans-blood-brain barrier delivery of Mn-$TPPP_4$, the results presented here provide a foundation for improvement and broader application of the technique in living animals.

DISCUSSION

We describe a new strategy for gene visualization by MRI, based on reporter enzyme-catalyzed precipitation and accumulation of an MRI contrast agent. This mechanism parallels successful strategies for gene product visualization by histology, but has not previously been applied for reporter protein detection by MRI. We showed that the secreted reporter enzyme SEAP directs dephosphorylation of the water soluble metalloporphyrin Mn-$TPPP_4$, which forms an insoluble green precipitate that is visible *in vitro* and by MRI in both sectioned and live tissue. The expected origin and specificity of the contrast changes is supported by detailed biochemical characterization and by *in vivo* experiments with control compounds and background phosphatase inhibition. We did not examine subcellular localization of the dephosphorylated Mn-$TPPP_4$ conversion products in tissue, but in an earlier study of intracerebrally injected metalloporphyrin probes, a weakly cationic complex similar to THPP were found to be predominantly cytosolic, as opposed to partitioned into membranous or nuclear compartments (Lee et al., 2010). In contrast, the relatively fast depletion of Mn-$TPPP_4$ and its analog Mn-$TPPS_4$ are consistent with a predominantly extracellular distribution. Our data do not demonstrate whether Mn-$TPPP_4$ cleavage products bind to proteins, lipids, or other hydrophobic components of the tissue, but it is possible that such interactions contribute to the apparent relaxivity and perhaps also to the retention of hydrophobic metalloporphyrins *in vivo*.

Because of the optical activity of the dephosphorylated Mn-$TPPP_4$ products, we were able to compare MRI scans with direct visualization of the accumulated metalloporphyrins in light microscopy. We could also compare results with histological staining for SEAP using the established BCIP-NBT method (Stoker and Bissell, 1987). Excellent agreement was found in *ex vivo* brain samples obtained from rats infected with targeted infusion of viral vectors carrying the SEAP gene. Homogeneous exposure to Mn-$TPPP_4$ across entire brain samples led to well defined contrast enhancement only near areas expressing SEAP, corresponding closely to BCIP-NBT results. In initial *in vivo* experiments, intracranially-injected Mn-$TPPP_4$ also stained SEAP-expressing brain areas more effectively than control areas.

The MRI signal changes we reported in tests of the SEAP reporter detection method approached 100% *ex vivo* (Figure 3) and 40% *in vivo* (Figure 4). These differences were obtained using strong viral expression of SEAP and delivery of substantial amounts of substrate (~0.5 mM Mn-$TPPP_4$), but further applications of the method might involve lower levels of reporter expression or substrate delivery. If necessary to boost signal, repeated substrate infusions could be applied, making use of the outstanding stability of SEAP/PLAP expression *in vivo* (Wang et al. 2001). Further improvements to the reporter visualization technique might also be accessible through protein engineering of the enzyme or the design of altered substrates with increased product relaxivity, better turnover, or greater specificity for SEAP. For experiments in living brains, an additional obvious area for improvement will be the development of a strategy for homogeneous trans-blood-brain barrier (BBB) delivery of SEAP substrates (Lelyveld et al., 2010). Ultrasound (US)-mediated BBB disruption has been shown to deliver MRI-detectable contrast agents to rodent brains (Vykhodtseva et al., 2008), in some cases spatially homogeneously (Howles et al., 2010), and may be an ideal technique for this purpose. Agents of widely varying sizes can be delivered using US-mediated disruption, and porphyrin agents similar to Mn-$TPPP_4$ appear to be amenable to this technique as well (unpublished results). A second BBB disruption technique, mannitol-mediated hyperosmotic shock (Neuwelt and Rapoport, 1984), has also been used for MRI contrast agent delivery, and could be useful in the future. It should be noted that for putative applications outside the brain, SEAP reporter imaging with Mn-$TPPP_4$ might not require special delivery techniques, however. A further area where the need for BBB permeability might be avoided is in applications to *ex vivo* neuroimaging and MRI microscopy. *Ex vivo* results in Figure 3 show quite strong and enzyme-specific contrast by the standards of current MR-based gene imaging strategies, obviously facilitated by the fact that SEAP substrate Mn-$TPPP_4$ could be washed homogeneously over all areas of the tissue, as well as by the reduction of background phosphatase activity due to histological processing. Similar application of this Mn-$TPPP_4$/SEAP staining method in conjunction with other anatomical or analyte-sensitive contrast techniques might have utility for understanding aspects of tissue structure and function by MRI.

In an explicit comparison with previously introduced MRI-based strategies for gene reporter imaging, the SEAP/Mn-$TPPP_4$ strategy may offer both strengths and weaknesses. Like most other enzyme-based reporter strategies (Hsieh and Jasanoff, 2012), the method presented here requires a synthetic, exogenous substrate, an obvious disadvantage compared with MRI gene reporters based on endogenous metal accumulation (Bartelle et al., 2012; Cohen et al., 2005; Genove et al., 2005). Because the SEAP substrate is not a biological molecule, however, it is not subject to regulation by biological mechanisms, and may provide greater contrast. Compared with other MRI enzyme reporter systems, detection of SEAP is facilitated by the fact that the reporter enzyme is extracellular rather than cytosolic (Matsushita et al., 2012; Westmeyer et al., 2010). The fact that contrast in the SEAP imaging method is due to probe accumulation *vs.* relaxivity changes may also present an advantage (Olson et al., 2010; Weissleder et al., 2000). Only probes modified by the reporter enzyme accumulate and induce contrast enhancements, whereas unmodified probes wash away within a day or so. Importantly, this avoids the need to distinguish differences in probe concentration from differences in relaxivity—a problem associated with many MRI reporter

systems in which responsive enzymatic substrates are used. Compared with chemical exchange saturation transfer (CEST) agents designed to respond to enzymes (Airan et al., 2012; Li et al., 2011; Liu et al., 2011; Yoo and Pagel, 2006), T_1 contrast-based systems have the disadvantage of being more difficult to analyze quantitatively; determining the amount of probe accumulation is not possible without knowledge of the background T_1, which in most cases would best be measured before Mn-TPPP$_4$ delivery. On the other hand, the T_1 contrast mechanism probably offers greater signal-to-noise ratio, and the solubility switch mechanism applied here could also be adapted to promote accumulation of a CEST agent if desired.

A significant benefit of the SEAP/Mn-TPPP$_4$ system for applications in animals is the possibility of combined MRI and optical readouts from stained tissue (Lee et al., 2010). Here this is achieved using a single paramagnetic chromophore platform, so separation of moieties used for dual modality imaging in chemical conjugate contrast agents is not a potential problem. This advantage is further complemented by the availability of an additional MRI readout for SEAP activity (Westmeyer et al., 2010), plus the possibility of using fluorescent and luminescent substrates that could make multimodal imaging with this enzyme a tractable possibility (Berger et al., 1988). Transgenic reporter mice expressing membrane-bound PLAP to label specific neuronal subpopulations are also available (Badea et al. 2009) and may provide improved spatial localization of multimodal enzyme activity detection, compared with the secreted reporter enzyme used in the present study. Although further work is required to demonstrate robust *in vivo* imaging with SEAP, both specific molecular aspects of the strategy introduced here and general approach of directing an MRI enzyme reporter to catalyze probe accumulation via a solubility switch could inspire further studies in living animals.

SIGNFICANCE

We have presented a novel approach to genetic reporter imaging by MRI, in which a synthetic water soluble contrast agent, Mn-TPPP$_4$, undergoes cleavage and localized precipitation in the vicinity of an extracellular enzyme, SEAP. The accumulation-based contrast mechanism has potentially higher dynamic range than reporter imaging methods based on relaxivity changes, and optical absorbance of the porphyrin-based contrast agent enables direct comparison of results obtained by MRI and histology. Robust *ex vivo* reporter mapping was achieved using the SEAP/Mn-TPPP$_4$ system in virally-infected rat brain slices, and initial *in vivo* experiments demonstrate that injected Mn-TPPP$_4$ also produces substantial T_1-weighted MRI contrast enhancements in areas where SEAP is expressed. Brain applications of the SEAP/Mn-TPPP$_4$ reporter imaging approach could be extended in conjunction with trans-BBB delivery techniques. The results demonstrate advantages of optically active porphyrin-based MRI contrast agents for multimodal molecular imaging. The more general idea of using an extracellular transgene product to catalyze a switch in the solubility of a diffusible small molecule contrast agent may prove valuable for future MRI-based reporter imaging incorporating SEAP or other enzymes.

EXPERIMENTAL PROCEDURES

Reagents and supplies

Chemicals including solubilized placental alkaline phosphatase (PLAP) were obtained from Sigma-Aldrich (St. Louis, MO) unless otherwise noted. Mn-THPP, Mn-$TPPS_4$, and Mn-$TPPP_4$ were obtained from Frontier Scientific (Logan, UT). Adeno-associated serotype 9 (AAV9) viral vectors were prepared by Virovek Inc. (Hayward, CA).

Animal subjects

Male Sprague Dawley rats (250–300 g) were purchased from Charles River Laboratories (Wilmington, MA). After arrival, animals were housed and maintained on a 12 hour light/dark cycle and permitted *ad libitum* access to food and water. All procedures were performed in strict compliance with the Committee on Animal Care (CAC) guidelines of Massachusetts Institute of Technology.

Enzymatic Conversion of Mn-$TPPP_4$

Different concentrations of Mn-$TPPP_4$ (6–191 μM) were incubated at 37 °C with 0.01 units of SEAP or the equivalent amount of BSA (one unit is defined as the amount of enzyme that will hydrolyze 1 μmol of 4-nitrophenyl phosphate per minute at pH 10.4 and 37 °C). Samples were subsequently spun down for 30 min. at 20,000 × *g* and photographed to document different amounts of precipitate. Spectra were acquired on a SpectraMax M2 plate reader (Molecular Devices, Sunnyvale, CA) and data were exported into Matlab (Mathworks, Natick, MA) for processing and plotting.

Liquid chromatography-mass spectrometric analysis

Mn-$TPPP_4$ (0.5 mM) was incubated with PLAP (300 mU) at 37 °C (50 mM Tris, 1 mM $MgCl_2$, pH 9) and the reaction stopped with trifluoroacetic acid (10 μL TFA) at the time points indicated in Figure S2A. High performance liquid chromatographic (HPLC) separation was performed with a 1290 Infinity HPLC system using an Eclipse C-18 analytical scale column (Agilent Technologies, Santa Clara, CA) with gradients ranging from 30–100% acetonitrile with 0.1% TFA. Flow rate was 0.6 mL/min and injection volume was 2.5 μL. Mass spectrometric evaluation was accomplished on a Citius high resolution time-of-flight mass spectrometer from Leco Corporation (St. Joseph, US). Electrospray ionization was performed in positive ionization mode with a mass range from 100 to 2000 atomic mass units. Mass calibration was achieved by periodic co-infusion of the ESI-L Low Concentration Tuning Mix from Agilent. Tuning compound mass accuracies were in the range of 0.01–0.34 ppm and resolutions were between 30–60 (mass/full width at half peak height). Solvents for LCMS procedures were obtained from J. T. Baker (Deventer, Netherlands).

Cell culture experiments

HEK293 cells were transiently transfected using Lipofectamine 2000 (Life Technologies, Grand Island, NY) with constructs coding for SEAP (pSEAP2-Control, Clontech, Mountain View, CA). Two days after transfection, 13 μM Mn-$TPPP_4$ and 1 mM orthovanadate were

added in reduced serum media (Opti-Mem, Life Technologies) and incubated for 2.5 or 4.5 hours. Supernatants were subsequently arrayed into multititer plates and analyzed by spectroscopy and MRI.

Intracranial injections

To achieve thalamic expression of SEAP, Sprague-Dawley rats were positioned in a stereotaxic frame, anesthetized with isoflurane and implanted bilaterally with MRI compatible 26 gauge guide cannulae of 1.5 mm length (Plastics One, Roanoke, VA) that were stably fixated with dental cement. Injection cannulae (Plastics One) were connected via silicon-oil filled PE50 tubing to a syringe pump (PhD 2000, Harvard Apparatus, Hollis-ton, MA) and backfilled with solutions containing AAV9 viral particles at a titer of 7×10^{12} viral genomes (vg)/mL encoding mouse SEAP (Wang et al. 2001) driven by a cytomegalovirus (CMV) promoter. Injection cannulae were inserted into the guide cannulae and lowered to the thalamic target region (2.5 mm lateral to midline, 6 mm below dura, −2.5 mm caudal to bregma). A volume of 3 μL of viral particles was injected at 0.1 μL/min; then the cannulae were moved up twice by 2 mm to inject an additional 3 μL each time. Control injection sites received AAV9 encoding CMV promoter-driven GFP (1.5×10^{12} vg/mL) using an identical protocol. Injection cannulae were subsequently retracted slowly and replaced with dummy cannulae (Plastics One) that screwed firmly into the guide cannula pedestals. On the day of the first *in vivo* imaging experiment shown in Figure 4, the dummy cannulae were removed and an injection cannula inserted that was backfilled with the substrate (635 μM Mn-$TPPP_4$) solutions, 3 μL of which were injected into the same thalamic coordinate 6 mm below the dura, and another 3 μL at 4 mm below the dura. Injection cannulae were subsequently slowly retracted and replaced with dummy cannulae that were permanently sealed with dental cement. For the injection experiments shown in Figure S3, 4 μL of 0.5 mM Mn-$TPPS_4$ or Mn-THPP (solubilized at pH 14) in artificial cerebrospinal fluid (aCSF) were injected intracranially at 0.1 μL/min into the cortex (3.5 mm lateral to bregma, 2 mm below dura). For injection experiments shown in Figure S4, 1.5 mM Mn-$TPPP_4$ was delivered with or without 5 mM sodium orthovanadate. In this experiment, 1 μL aliquots of each sample were applied at three depths (3.5 mm, 3 mm and 2.5 mm and below dura), all with a with a flow rate of 0.1 μL/min.

Histology

Animals were perfused with 4% paraformaldehyde, brains extracted and sliced in 100 μm micrometer thin sections on a vibratome to prepare for colorimetric alkaline phosphatase assay. Sections were heated at 65 °C for 90 minutes in preheated phosphate buffered saline (PBS) and incubated with BCIP-NBT. Sections were subsequently washed briefly and mounted onto cover slides. Slides were scanned on a photo scanner at 600 dpi. Image contrast was linearly adjusted in Photoshop (Adobe Systems, Waltham, MA).

Magnetic resonance imaging

For *in vitro* measurements, samples were prepared as detailed above, arrayed into microtiter plates and placed in a 40 cm bore Bruker (Billerica, MA) Avance 4.7 T or 9.4 T MRI scanner. Unused wells were filled with buffer, and imaging was performed on a 1 mm slice

through the sample. A spin echo pulse sequence with repetition times (*TR*) ranging from 63 ms to 8 seconds was used (echo time *TE* was 8.5 ms, data matrices of 128 × 128 points). Images were reconstructed and relaxation rates calculated by exponential fitting using custom routines running in Matlab (Mathworks, Natick, MA). Dependence of relaxivity on pH was examined by comparing r_1 and r_2 values measured at 9.4 T and at pH 7 *vs.* pH 4.5. No significant differences were observed, with $r_1 = 6.1\ m^{-1}s^{-1}$ and $r_2 = 11\ m^{-1}s^{-1}$ at both pH values. Following incubation with 10 units of PLAP, apparent relaxivities of $r_1 = 1.37 \pm 0.01$ and $r_2 = 21.5 \pm 0.2\ m^{-1}s^{-1}$ were observed at pH 7; corresponding values measured one hour following acidification to pH 4.5 were $r_1 = 1.34 \pm 0.08\ m^{-1}s^{-1}$ and $r_2 = 23 \pm 1\ m^{-1}s^{-1}$, again indicating negligible effect of pH.

For *ex vivo* experiments, animals were perfused, the brains extracted and cut on a vibratome to sections of 100 μm thickness. The sections were then heated for 90 minutes at 65 °C in preheated PBS, followed by overnight incubation with 500 μM Mn-$TPPP_4$ in 100 mM Tris, pH 9.5. Following staining, slices were washed with PBS and embedded in mounting media. Embedded sections were scanned on a Bruker 9.4 T scanner, using a T_1-weighted two dimensional spin echo pulse sequence with 100 μm in-plane resolution (*TR*/*TE* = 100/12 ms). For *in vivo* experiments, animals were anesthetized with isoflurane, prepared for intracranial injections as described and positioned on a heated animal bed in a 4.7 T Bruker MRI scanner. Fast Low-Angle Shot (FLASH) images with *TR*/*TE*= 50/5 ms and 250 μm isotropic resolution were acquired approximately two hours after Mn-$TPPP_4$ injection and then on subsequent days. Data for Figure S3 were acquired with a fast spin echo (FSE) sequence with a RARE factor of four, *TR*/*TE* = 510/13 ms, and 210 μm in-plane resolution. MRI images were reconstructed using custom routines in Matlab. Coronal MRI slices from subsequent imaging days of each animal were spatially registered to the first imaging day using routines implemented in Matlab [Medical Image Registration Toolbox (Myronenko and Song, 2010)]. Region of interest (ROI) analysis for Figure 4 and Figure S4 was performed by positioning cylindrical ROIs over the bilateral injection sites (diameter of 1.5 and length of 1.75 mm, centered on the cannulae tips) and computing relative signal amplitudes, normalized by average signal in nearby control ROIs, ~3.5 mm lateral to injection sites, that did not receive substrate. ROIs for Figure S4 were ellipses centered on the cannulae tips with 1.7 mm diameter in the coronal plane and 0.84 mm diameter along the rostrocaudal axis.

Supplementary Material

Refer to Web version on PubMed Central for supplementary material.

Acknowledgments

This work was funded by a Raymond and Beverly Sackler Foundation Award and NIH grant DP2-OD2441 (New Innovator Award) to AJ, as well as an MIT-Germany Seed Fund grant to AJ and GGW. The authors thank Xiao-an Zhang for helpful discussions, Anurag Mishra for advice and assistance with some of the compounds, and Tehya Johnson for technical support.

Abbreviations

aCSF	artificial cerebrospinal fluid
Mn-THPP	[Mn(III)-*meso*-tetrakis (4-hydroxyphenyl)porphyrin]
Mn-TPPP$_4$	[Mn(III)-*meso*-tetrakis(4-phosphophenyl)porphyrin]
Mn-TPPS$_4$	[Mn(III)-*meso*-tetrakis(4-sulfonatophenyl)porphyrin]
MRI	(magnetic resonance imaging)
PBS	(phosphate buffered saline)
PLAP	(placental alkaline phosphatase)
ROI	(region of interest)
TE	(echo time)
TR	(repetition time)
SEAP	(secreted alkaline phosphatase)

References

Airan RD, Bar-Shir A, Liu G, Pelled G, McMahon MT, van Zijl PC, Bulte JW, Gilad AA. MRI biosensor for protein kinase A encoded by a single synthetic gene. Magn Reson Med. 2012

Arena F, Singh J, Gianolio E, Stefania R, Aime S. beta-Gal gene expression MRI reporter in melanoma tumor cells. Design, synthesis, and in vitro and in vivo testing of a Gd(III) containing probe forming a high relaxivity, melanin-like structure upon beta-Gal enzymatic activation. Bioconjugate Chem. 2011; 22:2625–2635.

Avrameas S. Coupling of enzymes to proteins with glutaraldehyde. Use of the conjugates for the detection of antigens and antibodies. Immunochemistry. 1969; 6:43–52. [PubMed: 4975324]

Badea TC, Hua ZL, Smallwood PM, Williams J, Rotolo T, Ye X, Nathans J. New Mouse Lines for the Analysis of Neuronal Morphology Using CreER(T)/loxP-Directed Sparse Labeling. Plos One. 2009; 4:11.

Bartelle BB, Szulc KU, Suero-Abreu GA, Rodriguez JJ, Turnbull DH. Divalent metal transporter, DMT1: A novel MRI reporter protein. Magn Reson Med. 2012 Epub ahead of print.

Berger J, Hauber J, Hauber R, Geiger R, Cullen BR. Secreted placental alkaline phosphatase: a powerful new quantitative indicator of gene expression in eukaryotic cells. Gene. 1988; 66:1–10. [PubMed: 3417148]

Chen CW, Cohen JS, Myers CE, Sohn M. Paramagnetic metalloporphyrins as potential contrast agents in NMR imaging. FEBS Lett. 1984; 168:70–74. [PubMed: 6705923]

Cohen B, Dafni H, Meir G, Harmelin A, Neeman M. Ferritin as an endogenous MRI reporter for noninvasive imaging of gene expression in C6 glioma tumors. Neoplasia. 2005; 7:109–117. [PubMed: 15802016]

Cui WN, Liu L, Kodibagkar VD, Mason RP. S-Gal, a novel 1H MRI reporter for beta-galactosidase. Magn Reson Med. 2010; 64:65–71. [PubMed: 20572145]

DePrimo SE, Stambrook PJ, Stringer JR. Human placental alkaline phosphatase as a histochemical marker of gene expression in transgenic mice. Transgenic Res. 1996; 5:459–466. [PubMed: 8840529]

DiLella AG, Hope DA, Chen H, Trumbauer M, Schwartz RJ, Smith RG. Utility of firefly luciferase as a reporter gene for promoter activity in transgenic mice. Nucleic Acids Res. 1988; 16:4159. [PubMed: 3375079]

Fields-Berry SC, Halliday AL, Cepko CL. A recombinant retrovirus encoding alkaline phosphatase confirms clonal boundary assignment in lineage analysis of murine retina. Proc Natl Acad Sci U S A. 1992; 89:693–697. [PubMed: 1731342]

Genove G, DeMarco U, Xu H, Goins WF, Ahrens ET. A new transgene reporter for in vivo magnetic resonance imaging. Nat Med. 2005; 11:450–454. [PubMed: 15778721]

Goring DR, Rossant J, Clapoff S, Breitman ML, Tsui LC. In situ detection of beta-galactosidase in lenses of transgenic mice with a gamma-crystallin/lacZ gene. Science. 1987; 235:456–458. [PubMed: 3099390]

Gringeri CV, Menchise V, Rizzitelli S, Cittadino E, Catanzaro V, Dati G, Chaa-bane L, Digilio G, Aime S. Novel Gd(III)-based probes for MR molecular imaging of matrix metalloproteinases. Contrast Media Mol Imaging. 2012; 7:175–184. [PubMed: 22434630]

Howles GP, Bing KF, Qi Y, Rosenzweig SJ, Nightingale KR, Johnson GA. Contrast-enhanced in vivo magnetic resonance microscopy of the mouse brain enabled by noninvasive opening of the blood-brain barrier with ultrasound. Magn Reson Med. 2010; 64:995–1004. [PubMed: 20740666]

Hsieh V, Jasanoff A. Bioengineered probes for molecular magnetic resonance imaging in the nervous system. ACS Chem Neurosci. 2012; 3:593–602. [PubMed: 22896803]

Hudson PB, Brendler H, Scott WW. A simple method for the determination of serum acid phosphatase. J Urol. 1947; 58:89–92. [PubMed: 20249384]

Kawakami T, Igarashi S. Spectrophotometric determination of alkaline phosphatase and a-fetoprotein in human serum with 5, 10,,15,20-tetrakis(4-phosphonooxyphenyl)porphine. Analyst. 1995; 120:539–542.

Keliris A, Ziegler T, Mishra R, Pohmann R, Sauer MG, Ugurbil K, Engelmann J. Synthesis and characterization of a cell-permeable bimodal contrast agent targeting beta-galactosidase. Bioorg Med Chem. 2011; 19:2529–2540. [PubMed: 21459584]

Koenig SH, Brown RD 3rd, Spiller M. The anomalous relaxivity of Mn3+ (TPPS4). Magn Reson Med. 1987; 4:252–260. [PubMed: 3574059]

Lee T, Zhang XA, Dhar S, Faas H, Lippard SJ, Jasanoff A. In vivo imaging with a cell-permeable porphyrin-based MRI contrast agent. Chem Biol. 2010; 17:665–673. [PubMed: 20609416]

Lelyveld VS, Atanasijevic T, Jasanoff A. Challenges for Molecular Neuroimaging with MRI. Int J Imaging Syst Technol. 2010; 20:71–79. [PubMed: 20808721]

Lepage M, Dow WC, Melchior M, You Y, Fingleton B, Quarles CC, Pépin C, Gore JC, Matrisian LM, McIntyre JO. Noninvasive detection of matrix metalloproteinase activity in vivo using a novel magnetic resonance imaging contrast agent with a solubility switch. Mol Imaging. 2007; 6:393–403. [PubMed: 18053410]

Li Y, Sheth VR, Liu G, Pagel MD. A self-calibrating PARACEST MRI contrast agent that detects esterase enzyme activity. Contrast Media Mol Imaging. 2011; 6:219–228. [PubMed: 21861282]

Liu G, Liang Y, Bar-Shir A, Chan KW, Galpoththawela CS, Bernard SM, Tse T, Yadav NN, Walczak P, McMahon MT, et al. Monitoring enzyme activity using a diamagnetic chemical exchange saturation transfer magnetic resonance imaging contrast agent. J Am Chem Soc. 2011; 133:16326–16329. [PubMed: 21919523]

Louie AY, Huber MM, Ahrens ET, Rothbacher U, Moats R, Jacobs RE, Fraser SE, Meade TJ. In vivo visualization of gene expression using magnetic resonance imaging [In Process Citation]. Nat Biotechnol. 2000; 18:321–325. [PubMed: 10700150]

Matsushita H, Mizukami S, Mori Y, Sugihara F, Shirakawa M, Yoshioka Y, Kikuchi K. (19)F MRI monitoring of gene expression in living cells through cell-surface beta-lactamase activity. Chembiochem. 2012; 13:1579–1583. [PubMed: 22777922]

Myronenko A, Song X. Intensity-based image registration by minimizing residual complexity. IEEE Trans Med Imaging. 2010; 29:1882–1891. [PubMed: 20562036]

Nakane PK, Pierce GB Jr. Enzyme-labeled antibodies: preparation and application for the localization of antigens. J Histochem Cytochem. 1966; 14:929–931. [PubMed: 17121392]

Neuwelt EA, Rapoport SI. Modification of the blood-brain barrier in the chemotherapy of malignant brain tumors. Fed Proc. 1984; 43:214–219. [PubMed: 6692941]

Olson ES, Jiang T, Aguilera TA, Nguyen QT, Ellies LG, Scadeng M, Tsien RY. Activatable cell penetrating peptides linked to nanoparticles as dual probes for in vivo fluorescence and MR imaging of proteases. Proc Natl Acad Sci U S A. 2010; 107:4311–4316. [PubMed: 20160077]

Stoker AW, Bissell MJ. Quantitative immunocytochemical assay for infectious avian retroviruses. J Gen Virol. 1987; 68:2481–2485. [PubMed: 2821185]

Tu C, Osborne EA, Louie AY. Activatable T(1) and T(2) magnetic resonance imaging contrast agents. Ann Biomed Eng. 2011; 39:1335–1348. [PubMed: 21331662]

Vykhodtseva N, McDannold N, Hynynen K. Progress and problems in the application of focused ultrasound for blood-brain barrier disruption. Ultrasonics. 2008; 48:279–296. [PubMed: 18511095]

Wang M, Orsini C, Casanova D, Millán JL, Mahfoudi A, Thuillier V. MUSEAP, a novel reporter gene for the study of long-term gene expression in immuno-competent mice. Gene. 2001; 279:99–108. [PubMed: 11722850]

Weissleder R, Moore A, Mahmood U, Bhorade R, Benveniste H, Chiocca EA, Basilion JP. In vivo magnetic resonance imaging of transgene expression. Nat Med. 2000; 6:351–355. [PubMed: 10700241]

Westmeyer GG, Durocher Y, Jasanoff A. A secreted enzyme reporter system for MRI. Angew Chem, Int Ed Engl. 2010; 49:3909–3911. [PubMed: 20414908]

Westmeyer GG, Jasanoff A. Genetically controlled MRI contrast mechanisms and their prospects in systems neuroscience research. Magn Reson Imaging. 2007; 25:1004–1010. [PubMed: 17451901]

Yao Z, Borbas E, Lindsey JS. Soluble precipitable porphyrins for use in targeted molecular brachytherapy. New J Chem. 2007; 32:436–451.

Yoo B, Pagel MD. A PARACEST MRI contrast agent to detect enzyme activity. J Am Chem Soc. 2006; 128:14032–14033. [PubMed: 17061878]

Zhang XA, Lovejoy KS, Jasanoff A, Lippard SJ. Water-soluble porphyrins as a dual-function molecular imaging platform for MRI and fluorescence zinc sensing. Proc Natl Acad Sci U S A. 2007; 104:10780–10785. [PubMed: 17578918]

HIGHLIGHTS

- An alkaline phosphatase reporter catalyzes precipitation of paramagnetic phosphoporphyrins
- Enzymatic product accumulation is visible by light microscopy and magnetic resonance imaging
- The MRI contrast mechanism detects virally-driven phosphatase expression *ex vivo* and *in vivo*

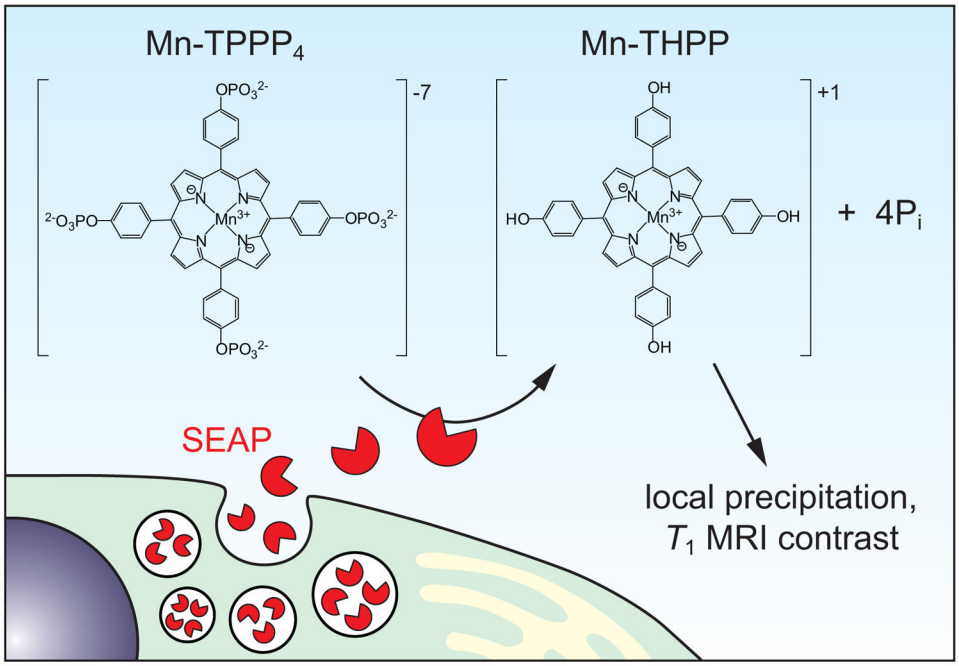

Figure 1. Schematic of the SEAP/Mn-TPPP$_4$ reporter approach

The secreted alkaline phosphatase reporter enzyme (SEAP, red) is produced by genetically modified cells and acts on the MRI contrast agent Mn-TPPP$_4$ (structure shown), cleaving up to four phosphates and inducing precipitation of the products, which have low solubility compared with Mn-TPPP$_4$. Accumulation of dephosphorylated contrast agents leads to local increases in T_1-weighted MRI contrast in the vicinity of cells expressing SEAP.

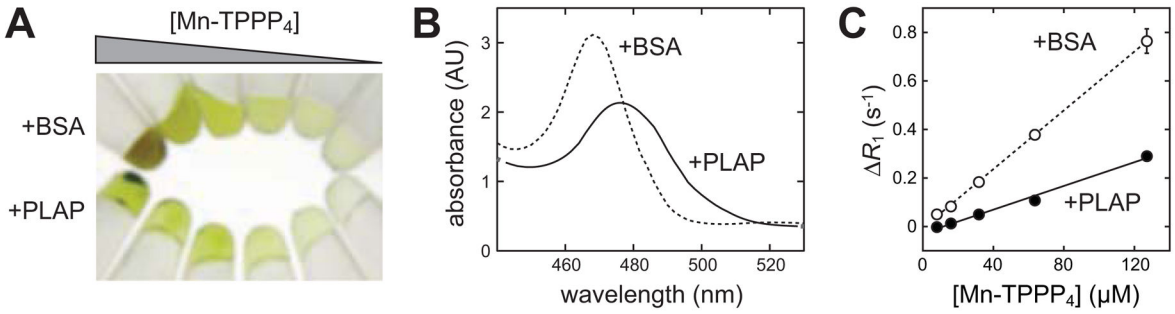

Figure 2. Action of PLAP on Mn-TPPP$_4$

(A) Solutions of Mn-TPPP$_4$ ranging from 6 to 191 μM in factors of two were incubated with 0.01 units of PLAP (bottom row) or an equivalent amount of BSA (top row) in 100 μL microtiter wells, centrifuged after 30 minutes, and photographed in Eppendorf tubes. Concentration-dependent build up of precipitate is visible in the SEAP but not the BSA condition. **(B)** Action of PLAP on Mn-TPPP$_4$ also induces a shift in the absorbance spectrum of the porphyrin. Here spectra were obtained from samples following incubation of 1 unit of SEAP or 1 nmol BSA for 30 minutes with 70 μM Mn-TPPP$_4$. **(C)** The effect of varying concentrations of Mn-TPPP$_4$ on the T_1 relaxation rate of buffered saline solutions was assessed in the presence of 0.01 units SEAP or 10 pmol BSA. The difference in R_1 from background (ΔR_1) is linear as a function of Mn-TPPP$_4$ concentration and shows an expected decrease in the ΔR_1 following dephosphorylation and reduction in solubility of the contrast agent.

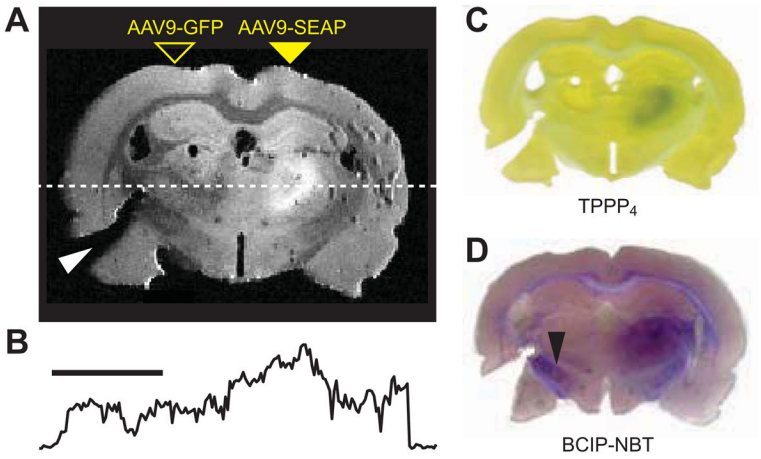

Figure 3. MRI microscopy of SEAP expression in an Mn-TPPP$_4$-stained brain slice

(A) T_1-weighted MRI scan of a 100 μm-thick brain slice from an animal infected with AAV9 viral vectors encoding SEAP or GFP (control) injected into right and left thalamus, respectively. The brain slice was notched (white arrowhead) purposefully to mark the control side. **(B)** A cross section through the image (dotted line in panel A) indicates the relative MRI signal across the slice; roughly twofold higher MRI signal is observed in SEAP expressing region. **(C)** Light micrograph of the section imaged in panel A, showing dark green staining in the region of greatest contrast agent accumulation and MRI contrast. **(D)** A neighboring brain slice stained with the BCIP-NBT method to map SEAP by conventional histology shows a clear focus of heightened phosphatase activity centered around the area of AAV9-SEAP infection and contrast agent accumulation. Some likely nonspecific staining is also apparent (black arrowhead).

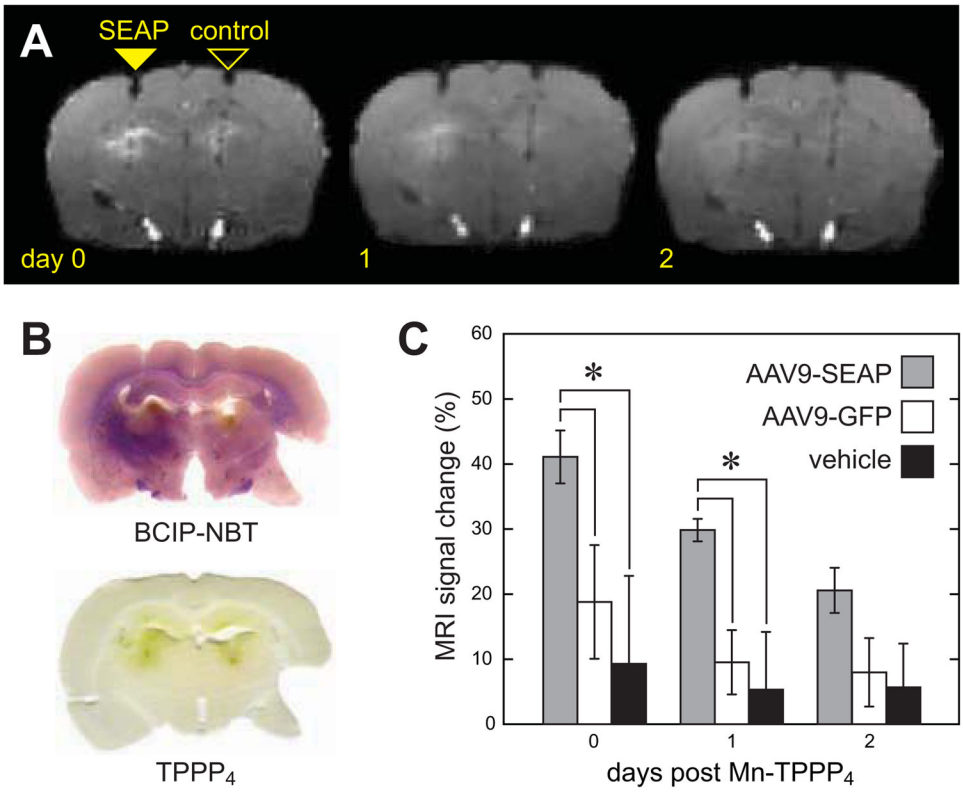

Figure 4. Mn-TPPP$_4$ induces amplified contrast in areas of SEAP expression *in vivo*

(A) MRI scans obtained over three days from an animal infected with AAV9-SEAP (left) and AAV9-GFP (control, right) and treated with identical infusions of Mn-TPPP$_4$ at the injection sites. T_1 contrast at the SEAP site is higher than the control on day 0 (approximately 2 hours after contrast agent delivery) and persists with diminishing amplitude over subsequent imaging sessions. **(B)** The brain from panel A was perfused and sectioned following scanning. Sections from near the injection sites were stained with BCIP-NBT to reveal phosphatase activity (top) and left unstained to reveal intrinsic porphyrin absorbance. **(C)** Group data from AAV9-SEAP (n = 5) and control injections of AAV9-GFP (n = 3) or vehicle (n = 2) injection sites, showing persistently higher Mn-TPPP$_4$ staining on the three days including and following the day of contrast agent delivery, which was statistically significant with respect to both controls with t-test $p < 0.04$ and $p < 0.02$ on days 0 and 1, respectively.